IMPACT OF THE VARIATION OF THE RECEIVER GLASS ENVELOPE TRANSMITTANCE AS A FUNCTION OF THE INCIDENCE ANGLE IN THE PERFORMANCE OF A LINEAR FRESNEL COLLECTOR

José A. López-Alvarez[1], Miguel Larraneta[1], Manuel A. Silva-Pérez[2], Isidoro Lillo-Bravo[2]

[1] Andalusian Association for Research and Industrial Cooperation (AICIA)

[2] University of Seville. Spain

Corresponding author:

Miguel Larraneta. Camino de los Descubrimientos s/n, 41092 Seville, Spain. Phone number: (+34)954487237

E-mail: mlarraneta@gter.es

Abstract

In this paper, we focus on the variation of the transmittance of the receiver glass envelope as a function of the incidence angle and we measure its impact on the annual optical efficiency of a LFR plant using ray-tracing techniques. For this purpose, we draw up a detailed model of the LFR collector installed on the roof of the School of Engineering of the University of Seville, Spain. We also calculate the optical efficiency with and without a secondary reflector and with constant or variable transmittance receiver glass envelope properties.

We run simulations using a clear-sky annual 1-min synthetic data set as input and calculate an average annual optical efficiency using efficiency matrices and Incidence Angle Modifiers (IAM) obtained from ray-tracing simulations. We find that the effect of the variation of the receiver glass envelope optical properties, as a function of the incidence angle, reduces the annual optical efficiency by 2.5%when the LFR plant has a basic secondary reflector and by 0.7% when there is no secondary reflector, according to the results obtained when using constant optical properties. We also evaluate the performance of the system with an optimised secondary reflector design.

Glossary

LFR: Lineal Fresnel Reflector

IAM: Incidence Angle Modifiers

PTC: Parabolic Trough Collectors

Θ: Incidence angle

DNI: Direct Normal Irradiance

m_R : Relative Air Mass

I_{CS}: Solar Constant

E_0: Correction due to Earth-Sun distance

°N: North

°W: West

LiBr: Lithium Bromide

P_{abs}: Power impinging on the absorber tube

η_{opt}: Optical efficiency

A_{cap}: Solar field aperture

ψ: Solar azimuth

α: Solar elevation

IAM: Incident Angle Modifier

IAM_l: Longitudinal Incident Angle Modifier

IAM_t: Transversal Incident Angle Modifier

η_o: Optical efficiency when the sun is at the zenith

τ: Transmissivity

E_{rec}: Total energy impinging the receiver

DNI_{CSY}: Clear sky DNI

$\eta_{opt_{average}}$: Annual average optical efficiency

Keywords

Linear Fresnel, Optical properties, Ray tracing.

1 Introduction

A Linear Fresnel Reflector (LFR) is a solar collector that reflects the sun rays onto a fixed linear receiver that stands along and above the reflectors. It uses long, flat or slightly curved mirrors to reflect the sunlight. The LFR is a promising technology and an attractive option because of its simplicity and its relatively low construction cost [1]. Usually, Fresnel solar collectors are compared with Parabolic Trough Collectors (PTC) for medium temperature applications. Many researchers state the advantages of using the LFR over the PTC [2-5], identifying the elimination of the problems derived from the movement of the receiver [6] and the reduction on the operation and maintenance costs [7] as the most significant advantages. However, the optical efficiency of the LFR is lower than the optical efficiency of the PTC [8].

LFR collectors provide thermal energy in the medium temperature range (100-300 ºC), making it a promising technology in fulfilling the demand of the majority of industrial processes [9]. Other applications of thermal energy in the medium temperature range are electricity production [10], solar cooling [11] and solar desalination [12].

In recent years, some studies related to the optimisation of the optical, thermal and geometrical parameters of different LFR configurations have been carried out [13-14]. Optical optimisation can be performed using analytical methods [15], integral methods, nonimaging optics techniques [16] and especially Monte Carlo-based ray-tracing techniques that provide great accuracy and flexibility [17-18].

Ray-tracing methods are widely used to analyse and optimise the geometrical performance of LFR. Zhu evaluates the impact of adjusting the tilt of the collector according to the solar elevation angle [19] and designs a stretched parabolic linear Fresnel reflector [20] using Tracepro ray-tracing software [21]. Pulido-Iparraguirre et al. [22] develop a ray-tracing code to optimise the solar collector size, tilt and orientation, and the receiver design. However, none of the methods used consider the impact of the variation of the optical properties such as the reflectance and transmittance of the receiver glass envelope as a function of the incidence angle (θ). It is common practice to adopt a constant value of reflectance and transmittance, but this assumption may lead to significant errors in the estimation of the optical efficiency of a LFR system.

In this research paper, we use Tonatiuh, an open source ray-tracing code specifically developed for the optical simulation of solar concentrators [23], to evaluate the impact of the angular dependence of the receiver glass envelope transmittance in a LFR plant. To that end, we model a real plant [24] installed on the roof of the School of Engineering of the University of Seville (Spain) and we run several ray-tracing simulations with constant and variable optical properties. We use a clear-sky DNI annual set and the average optical efficiency as a weighting factor for the location of Seville as a performance indicator. This research justifies the importance of using efficiency matrices and variable optical properties of the receiver glass envelope when simulating the performance of LFR plants.

This paper is structured as follows: section 2 presents the solar irradiation data used for the calculations, details the modelled LFR plant and describes the simulations. Section 3 shows the main results in terms of the optical efficiency on a monthly and annual basis, and a comparison with an improved secondary reflector design. Conclusions are then presented in Section 4.

2 Data and Methodology

This section includes the data used and the steps followed for simulating the optical performance of the modelled LFR plant.

2.1 Meteorological data

In this study, we use an annual set of clear-sky 1-min Direct Normal Irradiation (DNI) data. We perform an envelope method which is widely used for the estimation of the direct fraction index [25]. Any of the well-known clear-sky DNI models could be used; in this case, we use the A-B clear-sky model.

$$I_{bn_{cs}} = I_{cs} \cdot E_0 \cdot \frac{A}{1 + B \cdot m_R} \quad , \tag{1}$$

where m_R is the relative air mass I_{CS} is the solar constant, E_0 the correction due to Earth-Sun distance and *A* and *B* are empirical parameters intended to model the state of transparency or turbidity of the atmosphere. We calculate the A and B parameters by using an empirical fit from fourteen years of DNI measurements at the location of Seville (Spain) [26]. In Table 1 we present the main climatic characteristics of the selected location and the estimated couple of parameters defining the clear-sky envelope.

Table 1. Main climatic characteristics and couple of parameters defining the clear-sky envelope estimated for the location of Seville

Location	Latitude (°N)	Longitude (°W)	Altitude (m)	Climate	A	B
Seville	37.4	6	12	Mediterranean	0.862	0.136

2.2 Plant description

The LFR plant is a real hybrid solar cooling plant, which was installed in 2008 at the School of Engineering of the University of Seville in partnership with Gas Natural (Spanish natural gas and electrical energy utilities company) as a long-term project to boost the integration of both natural gas and solar energy in refrigeration applications (Fig. 1) [15]. The solar plant is coupled with a double effect LiBr + water absorption chiller with an auxiliary gas burner.

Fig. 1. General view of the modelled plant

The solar field longitudinal axis has a deviation of 12.05° with respect to the East-West direction and a total collector area of 352 m^2. It has 11 rows separated by a spacing of 20 cm, with 16 mirrors, 4 x 0.5 m^2 each, per row, and the total number of mirrors is 176. Each row is equipped with a solar tracking system.

The length of the solar field, as well as the receiver, is 64 m. The mirrors, with curvature radii between 8.6 and 10.6 m, have a nominal specular reflectance of 0.92. The receiver, a SCHOTT PTR® 70, is placed 4 m above the mirror plane. It is composed of a steel tube with a nominal absorptance of 0.94 and a glass envelope with a nominal transmittance of 0.96[1]. The secondary reflector is a thin metal parabola with a nominal reflectance of 0.77. We model the optical errors of the reflecting surfaces assuming a normal distribution with a standard deviation of 3.38 mrad. The working fluid is slightly subcooled liquid water at a nominal operating temperature of 180°C and a pressure of 13 bar.

The main characteristics of the solar field and the receiver are presented in Table 2. The main optical parameters of the solar facility are presented in Table 3.

Table 2. Main dimensional characteristics of the modelled LFR plant

Characteristic	Value	Unit
Solar field aperture	352	m^2

[1] This value is used in simulations with constant optical properties. In the case of simulations with variable optical properties, we use a value dependent on the incidence angle of the ray to the tube (Fig.3).

Solar field length	64	m
Orientation	East–West (approx.)	-
Number of rows	11	-
Mirror dimension	4 x 0.5	m^2
Mirror reflectance	0.92	-
Mirror curvature	8.6-10.6	m
Receiver length	64	m
Height of the receiver	4	m
Receiver model	SCHOTT PTR©70	-

Table 3. Main optical characteristicics of the modelled LFR plant

Characteristic	Value	Unit
Solar field mirror reflectance	0.92	-
Secondary reflector reflectance	0.77	-
Absorber tube absorptance	0.94	-
Receiver glass tube transmittance	0.96[1]	-
Solar field sigma slope	3.38	mrad

2.3 Ray-tracing model

We run several ray-tracing simulations of the LFR collector using the Tonatiuh code [27]. This Monte Carlo-based ray-tracing program for the optical simulation of solar concentrators has been experimentally validated in different plants [28-29]. In Tonatiuh, the rays are randomly thrown from a focus emulating the sun disk, and then are reflected, absorbed or refracted, depending on the optical characteristics of the elements of the system. Tonatiuh has an object-oriented graphical interface providing an extensive palette of surfaces. The geometry of the simulated system can be built up from a combination of simple elements defined by their geometrical and optical properties. Fig.2 shows the modelled plant seen through the Tonatiuh interface in the simulation for several stochastically distributed rays.

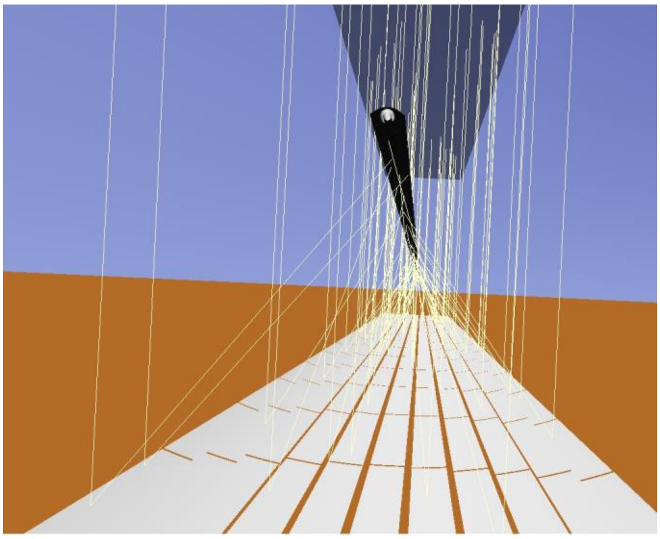

Fig. 2. Layout of the modelled LFR plant, seen through the Tonatiuh interface

The transmittance of the receiver glass envelope and the absorptance of the absorber tube are incidence angle dependent, although they are generally modelled as constant values. We can theoretically calculate the variation of the glass envelope transmittance as a function of the incidence angle following Snell's law and Fresnel equations. As can be observed in

Fig. **3.** Theoretical values of transmittance and reflectance of the receiver glass envelope as a function of the incidence angle.

, the theoretical results show that the transmittance and reflectance remain almost constant for solar incidence angles lower than 60° but drop drastically for incidence angles between 60° and 90°. We have considered a Buie sunshape [30] with a nominal value of 1000 W/m^2 and a circumsolar ratio of 2% for modelling purposes.

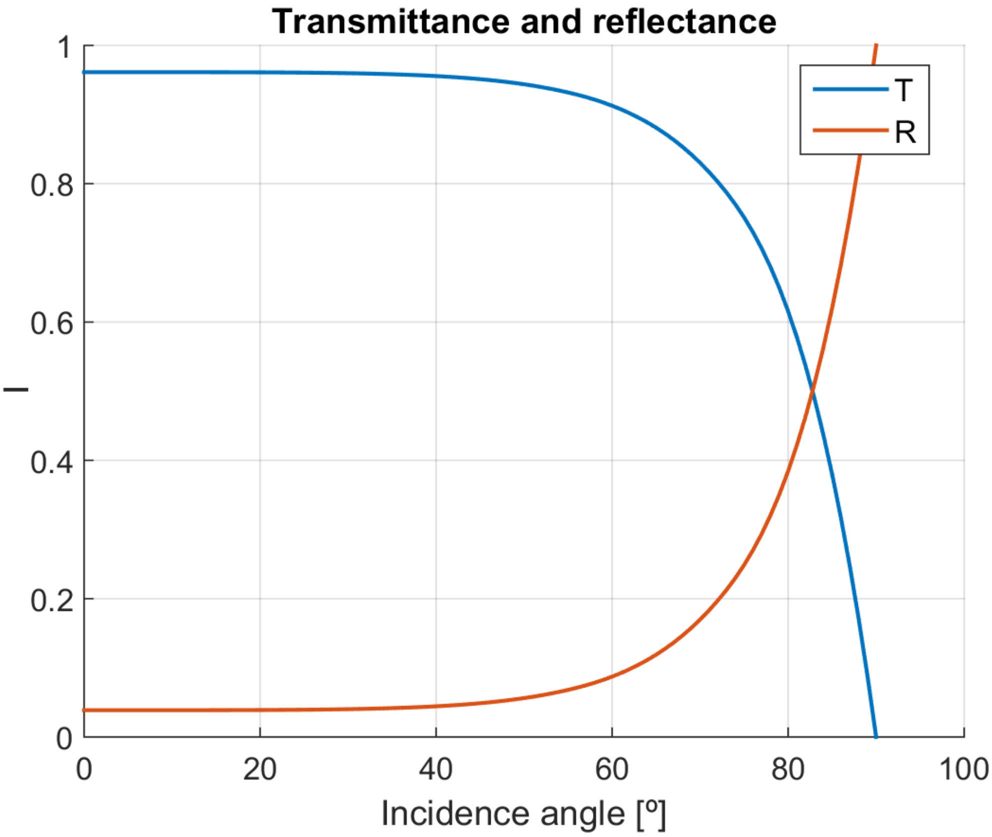

Fig. 3. Theoretical values of transmittance and reflectance of the receiver glass envelope as a function of the incidence angle.

From the simulations, we obtain the power impinging on the absorber tube[2], P_{abs}. The optical efficiency of the solar plant can be calculated as the ratio of P_{abs} to the available power on the solar field (primary):

$$\eta_{opt} = \frac{P_{abs}}{DNI \cdot A_{cap}} \quad , \qquad (2)$$

Where DNI is the direct normal irradiance and A_{cap} is the solar field aperture (352 m^2).

In this study, we use two different methods to describe the dependence of the optical efficiency on the sun's position. In the first method, the simulations cover the range of all possible solar positions, defined by the solar azimuth (ψ) and elevation (α) angles to obtain an optical efficiency matrix (see in **Fig. 7**). The second method is based on the concept of Incident Angle Modifier, IAM. The IAM is a practical and faster method to obtain the optical efficiency. The longitudinal IAM (IAM_l) is calculated by simulating the plant when the transverse angle is null, and the transverse IAM (IAM_t) is calculated by simulating the plant when the longitudinal angle is null. The optical efficiency can then be calculated for any solar position as:

$$\eta_{opt_{FIELD}} = \eta_o * IAM_l * IAM_t \ . \qquad (3)$$

[2] The optical properties of the absorber tube are also angular-dependent, but we have not considered this effect in our study. Therefore P_{abs} does not include the absorptance of the absorber tube.

Where η_o is the optical efficiency when the sun is at the zenith angle.

In Fig. 4, we present an Illustration of the solar-position-dependent collector at longitudinal and transversal angles [31].

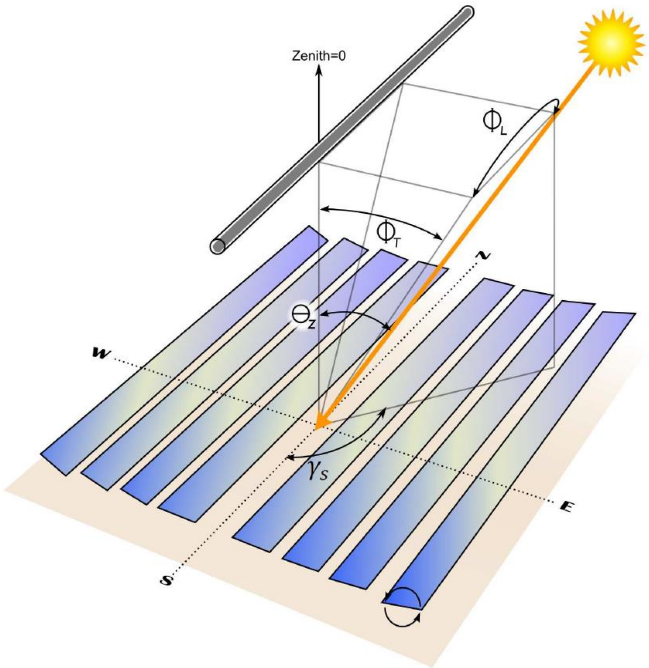

Fig. 4. Simple diagram of the solar-position-dependent collector at longitudinal and transversal angles [31].

3 Results

We run two different sets of simulations: one which takes into account a constant value of the receiver transmittance of 0.96 and another using an incidence angle-dependent transmittance value as shown in Fig.3. We also run simulations of the solar field including or removing the secondary reflector, leading to the four cases summarised in Table 4 and illustrated in Fig. 5.

Table 4. LFR simulations taken into account in this research

LFC simulations			
With secondary reflector		Without secondary reflector	
Constant receiver transmittance	Variable receiver transmittance	Constant receiver transmittance	Variable receiver transmittance
S1	S2	S3	S4

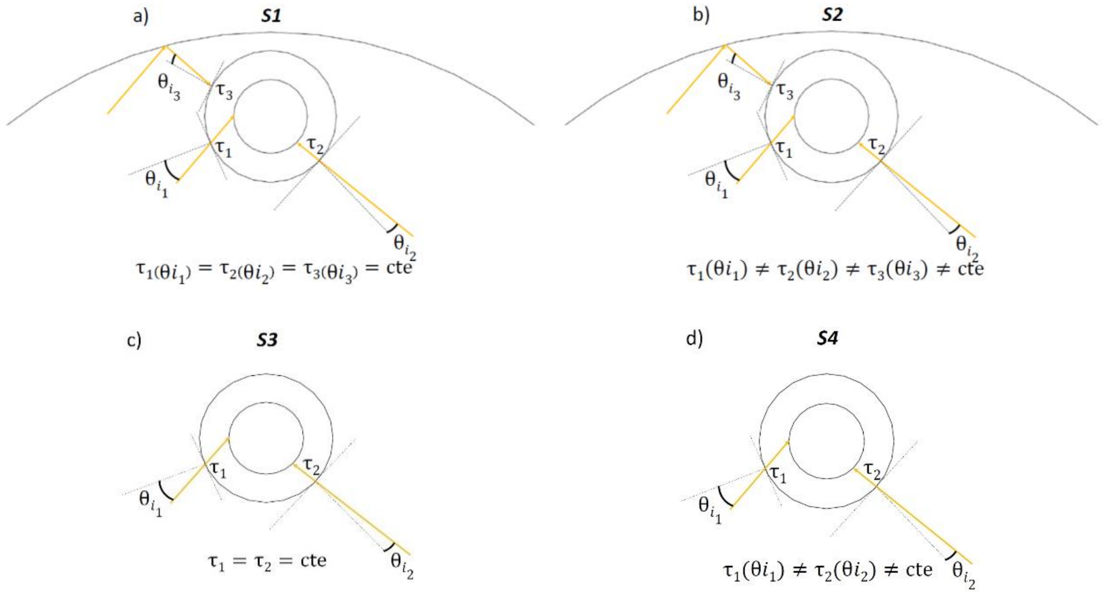

Fig. 5. Illustration of the LFR simulations modelled in this research.

S1 is the system with the secondary reflector and a constant value of the receiver transmittance. S2 is the system with the secondary reflector and considering an incidence angle-dependent transmittance value on the receiver. S3 is the system without the secondary reflector and a constant value of the receiver transmittance. S4 is the system without the secondary reflector and considering an incidence angle-dependent transmittance value on the receiver. The modelled secondary reflector is a perfect parabola with a width of 0.5 m and a focal length of 0.0884 m. The distance between the parabola vertex and the focal point is 0.08m. The inlet and outlet radii are 0.035 m and 0.0625 m respectively (Fig. 6).

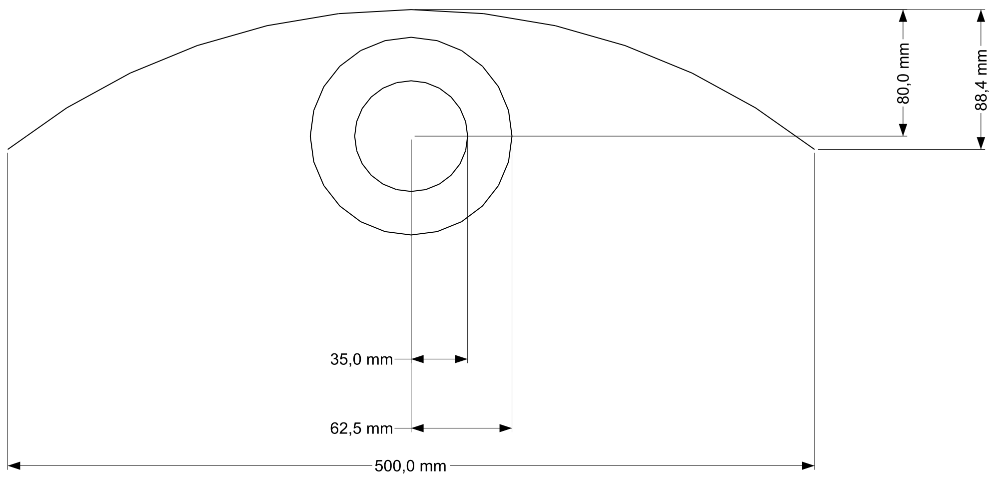

Fig. 6. Illustration of the modelled secondary reflector and receiver.

3.1 Annual optical efficiency

We calculate the optical efficiency for a number of solar positions defined by the solar azimuth and elevation angles, obtaining the efficiency matrix and the IAM profiles. In Fig. 7 and 8, we present the optical efficiency matrices as heat maps and the IAM curves for the four evaluated cases. The solar azimuth value of 90° corresponds to the East and 180° corresponds to the South. A solar elevation of 90° indicates that the sun is at the zenith angle.

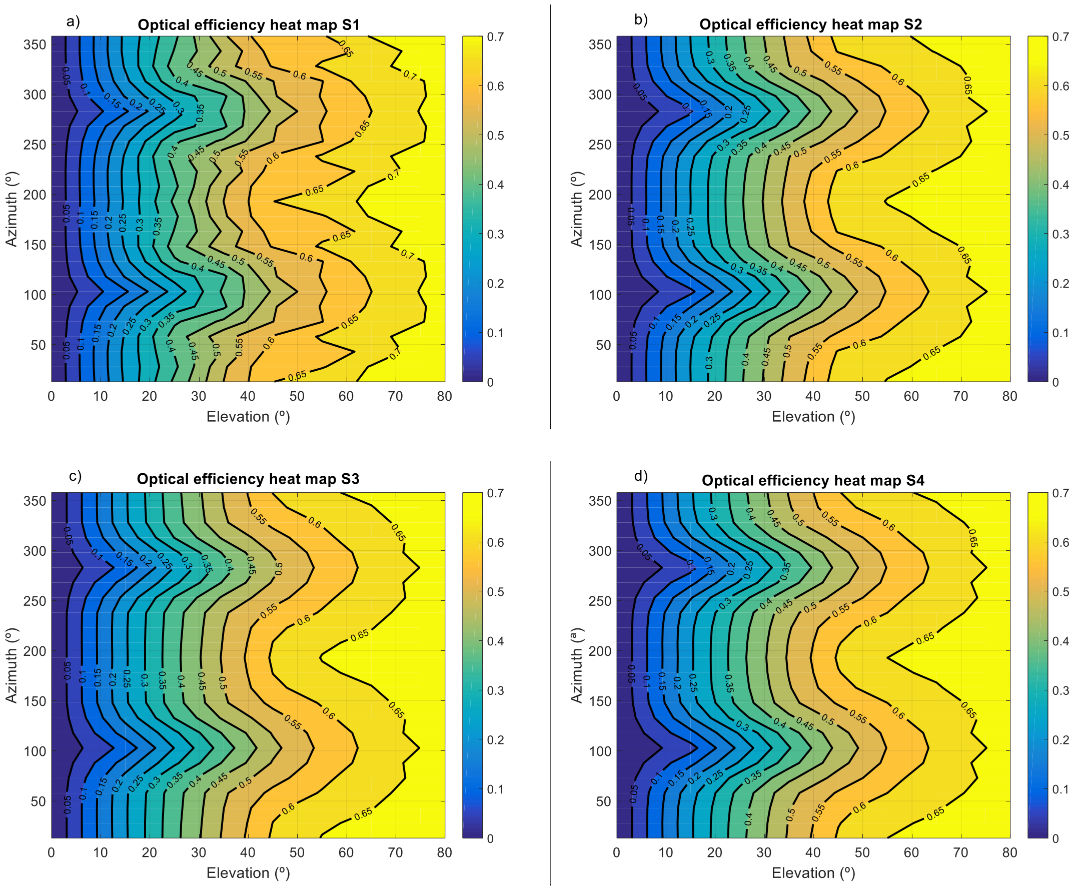

Fig. 7. Optical efficiency matrices presented as heat maps depending on the solar azimuth and elevation angles for the four evaluated cases.

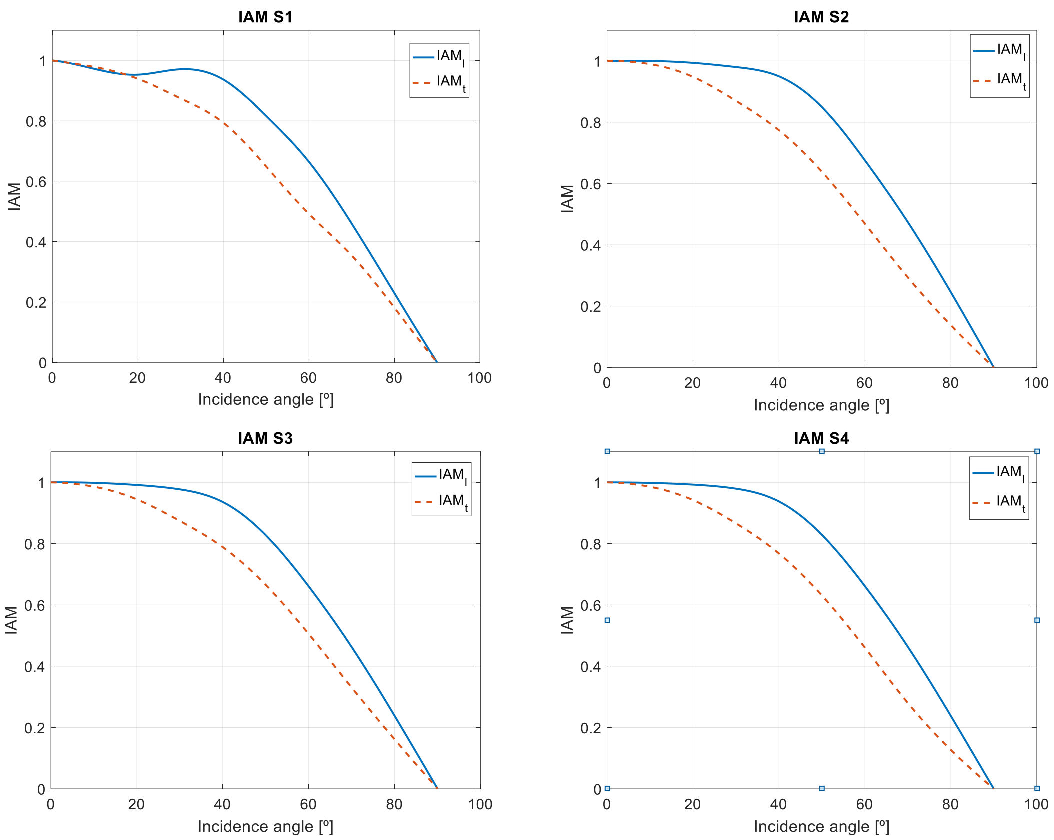

Fig. 8. Estimated IAM profiles for the four evaluated cases.

We then calculate the solar position for the location under study (Seville) in 1-min resolution for the entire year, and an optical efficiency value (η_{opt}) is assigned to each instant (i) from the efficiency matrix or the IAM profiles. The average optical efficiency is calculated as the quotient of the total energy impinging on the receiver (E_{rec}) to the total energy available in the solar field (E_{sf}). For a clear-sky year:

$$E_{rec} = \sum_{i=1}^{n} \left(\eta_{opt_i} \cdot \mathrm{DNI}_{CSY_i} \cdot A_{cap} \right) \quad , \tag{4}$$

$$E_{sf} = \sum_{i=1}^{n} \left(\mathrm{DNI}_{CSY_i} \cdot A_{cap} \right) \quad , \tag{5}$$

Where DNI_{CSY} is the clear-sky DNI and *i* is the time of the year in minutes (*n*=525600 for one year in the 1-min resolution).

$$\eta_{opt_{average}} = \frac{E_{rec}}{E_{sf}} \quad . \tag{6}$$

We calculate the annual average optical efficiency ($\eta_{opt_{average}}$) using the estimated efficiency matrices and the IAM profiles. The results for the annual optical efficiency obtained for the 4 cases considered are summarised in Table 5.

Table 5. Annual optical efficiency of the four evaluated cases calculated with the efficiency matrix and IAM methods.

	Annual optical efficiency ($\eta_{opt_{average}}$) [%]			
	With secondary concentrator		Without secondary concentrator	
	S1 τ=cte	S2 τ= τ(θ)	S3 τ=cte	S4 τ= τ(θ)
Efficiency matrix method	44.95	41.76	42.36	40.20
IAM method	42.40	39.29	39.91	38.58

The IAM method results in lower optical annual efficiency compared to the efficiency matrix method (≈-2.5%) for all the cases.

The use of a secondary concentrator implies an annual optical efficiency increase of 3.2%when taking into account constant receiver properties (S2 to S1) and 1.2% when taking into account the variation of the receiver properties (S4 to S3).

The impact of the use of variable optical properties of the receiver in the optical performance of the modelled systems is greater for the system with a secondary concentrator. The annual average optical efficiency decreases by approximately 2.5% from S1 to S3 and by 0.7% from S2 to S4.

These results suggest that a significant number of rays reflected on the secondary reflector impinge on the receiver glass envelope with a high incidence angle. We have calculated the distribution of the energy on the receiver discretizing into tree intervals depending on the incidence angle (θ ≤30°; 30°<θ ≤60°; 60°<θ ≤90°). Calculations have been carried out for systems with variable optical properties, with and without a secondary reflector (S2 and S4 respectively). Results are summarised in Table 6.

Table 6. Distribution of the energy on the receiver depending on the incidence angle for cases S2 and S4.

	Energy on the receiver (%)		
	θ ≤30°	30°<θ ≤60°	60°<θ ≤90°
S2	31.1	52.1	16.8
S4	31.5	51.9	16.6

In the case of the system with a secondary reflector, there is more energy on the receiver for large incidence angles and less energy for incidence angles lower than 30°.

3.2 Monthly optical efficiency

In the following, we will use the efficiency matrices for the calculations. We have calculated the average optical efficiency per month for the four evaluated cases. In Fig 9. We present the monthly optical efficiency for the constant properties (continuous blue line) and variable properties (dotted blue line) cases with a secondary reflector (left) and without a secondary reflector (right). In the secondary y-axes, we present the percentage differences calculated according to equations 6 and 7 (yellow lines).

$$Differences_{S1-S2}\,(\%) = \frac{\mathrm{S1} - \mathrm{S2}}{\mathrm{S1}} \cdot 100 \qquad (6)$$

$$Differences_{S3-S4}(\%) = \frac{\mathrm{S3} - \mathrm{S4}}{\mathrm{S3}} \cdot 100 \qquad (7)$$

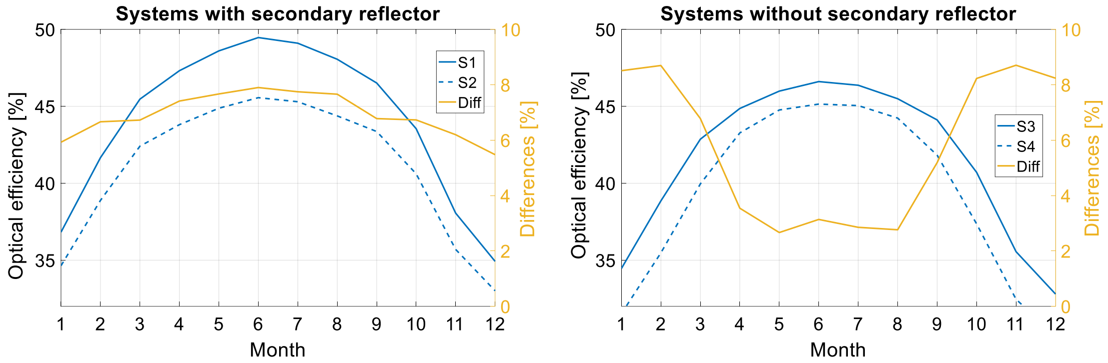

Fig. 9. Monthly optical efficiency of the four evaluated cases calculated with the efficiency matrices and differences found between constant and variable receiver glass envelope properties. Systems with a secondary reflector are presented on the left and those without it on the right.

When evaluating the monthly efficiency of the system with a secondary reflector (Fig 9. Left), we can observe that the differences found due to considering the constant or variable optical properties of the receiver glass envelope are greater in summer months reaching a maximum of 7.9% in June, when the solar elevation angles are higher. It should be noted that days are longer in the summer months in Seville. Hence, for the annual clear-sky DNI data set, most of the annual solar radiation is obtained in this period, coinciding with the greater differences in the optical efficiency. The average optical efficiency depends on the instantaneous optical efficiency as a weighting factor in the DNI, which in our case is the clear-sky DNI. In summer months, we find situations where we have a high solar radiation value with a low incidence angle more frequently than in winter. In the case of not using the secondary reflector (Fig 9. Right), differences are much lower for all the months, reaching a maximum of 3.4% in August. We also compare S1 to S3 and S2 to S4 for monthly efficiencies. In Fig 10 we present the monthly optical efficiency and their percentage differences calculated from equations 8 and 9 (yellow lines).

$$Differences_{S1-S3}\,(\%) = \frac{\mathrm{S1} - \mathrm{S3}}{\mathrm{S1}} \cdot 100 \qquad (8)$$

$$Differences_{S2-S4}(\%) = \frac{\mathrm{S2} - \mathrm{S4}}{\mathrm{S2}} \cdot 100 \qquad (9)$$

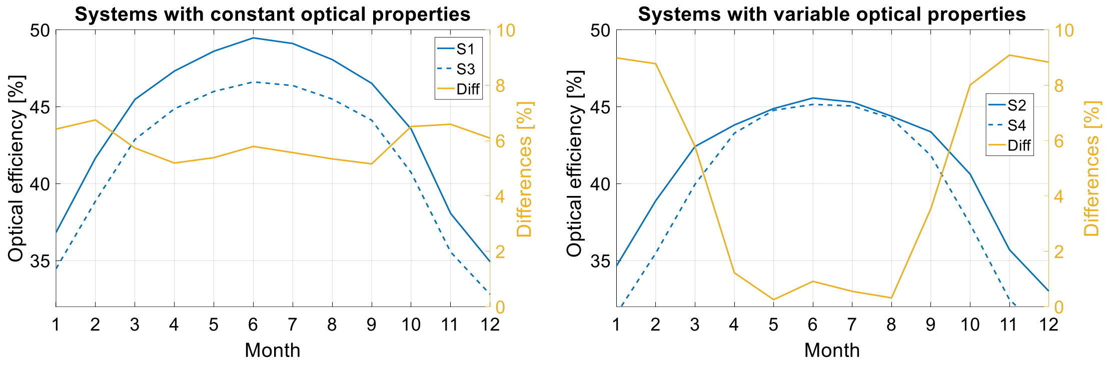

Fig. 10. Monthly optical efficiency of the four evaluated cases calculated with the efficiency matrix together with the differences found between them. Systems with constant optical properties are presented on the left and those with variable properties are on the right.

The monthly efficiency values are significantly lower in S3 than in S1 for all the months, but we find negligible differences between S4 and S2 in summer months, indicating a low contribution of the modelled secondary reflector in the energy obtained in the receiver when considering the variable transmittance of the receiver glass envelope.

4 Discussion

The main function of the secondary concentrator is to redirect rays that do not hit the receiver by increasing the number of rays that strike the receiver and therefore increasing the radiant energy impinging on it. Most of the rays reflected on the secondary concentrator hit the receiver with a high incidence angle (≥60°) leading to low transmittance values, which implies a lower flux on the receiver. In the case of not using a secondary reflector, all the rays come from the solar field. In these cases, the incidence angles are generally low (≤60°) and the receiver glass envelope transmittance almost reaches its maximum value.

Results suggest that the contribution of the installed secondary reflector is small when evaluating the modelled LFR plant with variable optical properties because the rays reflected on it impact the receiver glass envelope with large incidence angles, where the transmittance of the receiver glass envelope drops drastically. A number of authors have proposed alternative shapes of secondary reflectors in order to enhance the efficiency of LFR collectors [32]. The most promising secondary reflector design involves joining two sections of identical parabolas at the optical axis of the concentrator [33]. The dimensions of the two halves of the reflector are calculated using the radius of the absorber tube and the acceptance angle of the field. In Figure 11, we present the improved design of the secondary reflector for the modelled LFR plant.

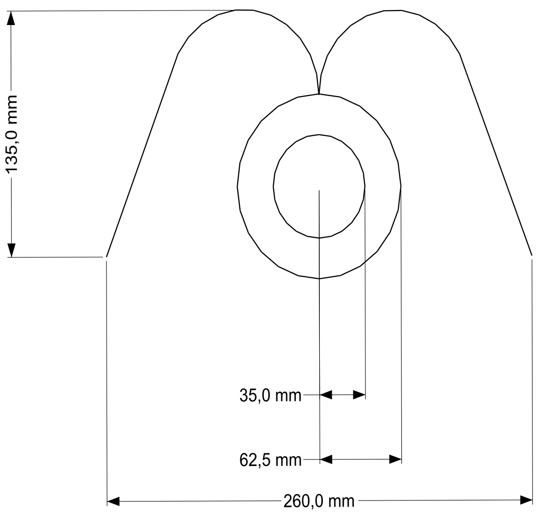

Fig. 11. Illustration of the improved secondary reflector together with the receiver.

We model the LFR plant including the improved secondary reflector (Fig. 11) instead of the basic secondary reflector (Fig. 6). We calculate the annual efficiency using the efficiency matrix method and taking into account constant optical properties of the receiver glass envelope (S5) or variable optical properties of the receiver glass envelope as a function of the incidence angle (S6). Results are summarised in Table 7

Table 7. Annual optical efficiency of the systems with the optimal secondary reflector, calculated using the efficiency matrix method.

	Annual optical efficiency ($\eta_{opt_{average}}$) [%]	
	S5	S6
Efficiency matrix method	45.82	45.31

There is a decrease of 0.5% from S5 to S6, that is, from constant to variable optical properties. The impact of the variation of the glass envelope transmittance as a function of the incidence angle when evaluating the improved secondary reflector design (Fig 11) is much lower than in the case of the basic design (Fig 6). We have also calculated the distribution of the energy on the receiver by discretizing into tree intervals according to the incidence angle. In Table 8, we present the distribution of the energy on the receiver for the case of S6. Results are compared to case S2.

Table 8. Distribution of energy on the receiver depending on the incidence angle. Comparison of cases S6 and S2.

	Energy on the receiver (%)		
	θ ≤30°	30°<θ ≤60°	60°<θ ≤90°
S6	33.5	53.1	13.4
S2	31.1	52.1	16.8

There is a significant drop of energy (-20%) impinging on the receiver for high incidence angles (60°<θ ≤90°), while for low incidence angles (θ ≤30°) there is a significant increase of energy (7.7%) impinging on the receiver.

5 Conclusions

To assess the effect of the incidence angle dependence of the receiver glass envelope transmittance on the performance of LFRs, we evaluated the optical performance of a LFR plant installed on the roof of the School of Engineering of the University of Seville using ray-tracing techniques. We have modelled the LFR plant in Tonatiuh and calculated the monthly and annual optical efficiency. Calculations have been performed considering constant and variable optical properties of the absorber tube glass envelope (transmittance and reflectance) as a function of the incidence angle. We have also estimated the optical efficiency of the LFR collector by removing the secondary collector and including an alternative improved shape of the secondary reflector. In light of the results, we can conclude that taking into account constant optical parameters of the absorber tube leads to significant overestimations of the energy produced by a LFR plant. The results of this study suggest that the optical efficiency estimations of LFR plants should be performed taking into account variable properties of the absorber tube glass envelope, mainly for LFR plants with basic secondary reflectors because most of the rays reflected by the secondary reflector impinge on the absorber tube with high incidence angles. When evaluating an improved secondary reflector design, the incidence angle dependence is less significant. In any case, the evaluation of secondary reflector designs should always be performed considering variable optical properties of the absorber tube glass envelope as a function of the incidence angle.

We have calculated the average optical efficiency using efficiency matrices and IAM methods, and we have found that the efficiency matrices method is a more accurate method than the IAM method for the optical efficiency calculation of a LFR plant. The IAM method implies an underestimation of the annual optical efficiency, which can be quantified as a reduction of 2.5% (from 42.5% to 40% on average in all the evaluated systems).

References

1. M. Lin, K. Sumathy, Y.J. Dai, R.Z. Wang, Y. Chen (2013). Experimental and theoretical analysis on a linear Fresnel reflector solar collector prototype with V-shaped cavity receiver. Applied Thermal Engineering. 5:1-2, 963-972.

2. Yanqing Zhu, Jifu Shi, Yujian Li, Leilei Wang, Qizhang Huang, Gang Xu, (2016). Design and experimental investigation of a stretched parabolic linear Fresnel reflector collecting system. Energy Conversion and Management, 126, 89-98.

3. Sudhansu S. Sahoo, Suneet Singh, Rangan Banerjee, (2016). Thermal hydraulic simulation of absorber tubes in linear Fresnel reflector solar thermal system using RELAP. Renewable Energy, 86, 507-516.

4. Hani H. Sait, Jose M. Martinez-Val, Ruben Abbas, Javier Munoz-Anton,(2015). Fresnel-based modular solar fields for performance/cost optimization in solar thermal power plants: A comparison with parabolic trough collectors. Applied Energy, 141, 175-189.

5. Lillo, I.; Pérez, E.; Moreno, S.; Silva, M. Process Heat Generation Potential from Solar Concentration Technologies in Latin America: The Case of Argentina. Energies 2017, 10, 383.
6. Shanmugapriya Balaji, K.S. Reddy, T. Sundararajan, (2016). Optical modelling and performance analysis of a solar LFR receiver system with parabolic and involute secondary reflectors. Applied Energy, 179, 1138-1151
7. Andreas Häberle , Christian Zahler, Hansjörg Lerchenmüller, Max Mertins, Christof Wittwer, Franz Trieb, Jürgen Dersch (2002). The Solarmundo line focussing Fresnel collector. Optical and thermal performance and cost calculations. Proc. SolarPACES, no. January, pp. 1–11
8. A.E. Rungasamy, K.J. Craig, J.P. Meyer, (2015). 3-D CFD Modelling of a Slanted Receiver in a Compact Linear Fresnel Plant with Etendue-Matched Mirror Field. Energy Procedia, 69, 188-197
9. Sven Werner. Norela Constantinescu. N. ECOHEATCOOL, the European Heat Market, 2016.
10. James Freeman, Klaus Hellgardt & Christos N. Markides (2015) An Assessment of Solar–Thermal Collector Designs for Small-Scale Combined Heating and Power Applications in the United Kingdom, Heat Transfer Engineering, 36:14-15, 1332-1347.
11. M.J. Tierney (2007). Options for solar-assisted refrigeration—Trough collectors and double-effect chillers. Renewable Energy, 32:2, 183-199.
12. Lourdes García-Rodríguez, Julián Blanco-Gálvez (212). Solar-heated Rankine cycles for water and electricity production: POWERSOL project. Desalination, 212:1-3, 311-318
13. Jie Zhu, Hulin Huang (2014). Design and thermal performances of Semi-Parabolic Linear Fresnel Reflector solar concentration collector. Energy Conversion and Management, 77, 733-737
14. María J. Montes, Rubén Barbero, Rubén Abbas, Antonio Rovira (2016). Performance model and thermal comparison of different alternatives for the Fresnel single-tube receiver. Applied Thermal Engineering, 104, 162-175.
15. F.J. Pino, R. Caro, F. Rosa, J. Guerra, (2013). Experimental validation of an optical and thermal model of a linear Fresnel collector system. Applied Thermal Engineering 50:2, 1463-1471
16. Ze-Dong Cheng, Ya-Ling He, Bao-Cun Du, Kun Wang, Qi Liang (2015). Geometric optimization on optical performance of parabolic trough solar collector systems using particle swarm optimization algorithm. Applied Energy, 148, 282-293.
17. Yu Qiu, Ya-Ling He, Ze-Dong Cheng, Kun Wang, (2015). Study on optical and thermal performance of a linear Fresnel solar reflector using molten salt as HTF with MCRT and FVM methods. Applied Energy, 146,162-173.
18. Ze-Dong Cheng, Xue-Ru Zhao, Ya-Ling He, Yu Qiu, (2018). A novel optical optimization model for linear Fresnel reflector concentrators. Renewable Energy, 129:A, 486-499
19. Yanqing Zhu, Jifu Shi, Yujian Li, Leilei Wang, Qizhang Huang, Gang Xu, (2017). Design and thermal performances of a scalable linear Fresnel reflector solar system. Energy Conversion and Management, 146, 174-181
20. Yanqing Zhu, Jifu Shi, Yujian Li, Leilei Wang, Qizhang Huang, Gang Xu, (2016). Design and

experimental investigation of a stretched parabolic linear Fresnel reflector collecting system. Energy Conversion and Management, 126, 89-98

21. TracePro User Manual; 2011.

22. Diego Pulido-Iparraguirre, Loreto Valenzuela, Juan-José Serrano-Aguilera, Aránzazu Fernández-García, (2019). Optimized design of a Linear Fresnel reflector for solar process heat applications. Renewable Energy, 131, 1089-1106

23. Blanco, M. J., Amieva, J. M., & Mancillas, A. (2005). The Tonatiuh Software Development Project: An open source approach to the simulation of solar concentrating systems. In ASME 2005 International Mechanical Engineering Congress and Exposition (pp. 157-164). American Society of Mechanical Engineers.

24. Pablo Bermejo, Francisco Javier Pino, Felipe Rosa (2010). Solar absorption cooling plant in Seville. Solar Energy, 84:8, 1503-1512

25. Skartveit, A., Olseth, J.A. The probability density and autocorrelation of short-term global and beam irradiance. Solar Energy 49 (1192), pp. 477-487.

26. Larrañeta-Gómez-Caminero, Miguel; M.J. Reno; Silva-Pérez, Manuel Antonio; Lillo-Bravo, Isidoro. 2017. Identifying periods of clear sky direct normal irradiance. Renewable Energy. 113:756–763.

27. Blanco, M. J., Amieva, J. M., & Mancillas, A. (2005, January). The Tonatiuh Software Development Project: An open source approach to the simulation of solar concentrating systems. In ASME 2005 International Mechanical Engineering Congress and Exposition (pp. 157-164). American Society of Mechanical Engineer

28. Blanco, M., Mutuberria, A., Monreal, A., & Albert, R. (2011). Results of the empirical validation of Tonatiuh at Mini-Pegase CNRS-PROMES facility. Proc SolarPACES.

29. Blanco, M. J., Mutuberria, A., & Martinez, D. (2010). Experimental validation of Tonatiuh using the Plataforma Solar de Almería secondary concentrator test campaign data. In Proceedings of the 16th Annual SolarPACES Symposium.

30. D. Buie, A.G. Monger, C.J. Dey. (2003). Sunshape distributions for terrestrial solar simulations. Solar Energy 74-2, pp. 113-122.

31. Michael J. Wagner, Guandong Zhu. 2012. A DIRECT-STEAM LINEAR FRESNEL PERFORMANCE MODEL FOR NREL'S SYSTEM ADVISOR MODEL. ESFuelCell2012-91317

32. R. Abbas, A. Sebastián, M.J. Montes, M. Valdés. 2018. Optical features of linear Fresnel Collectors with different secondary reflector technologies. Applied Energy 232, pp. 386-397

33. R. Oommen, S. Jayaraman. 2001. Development and performance analysis of compound parabolic solar concentrators with reduced gap losses – oversized reflector. Energy Conversion and Management 42, pp. 1379-1399